Research paper

Synthesis of mixed MOR/KOR efficacy cyclic opioid peptide analogs with antinociceptive activity after systemic administration

Renata Perlikowska [a], Justyna Piekielna [a], Luca Gentilucci [b], Rossella De Marco [b], Maria Camilla Cerlesi [c], Girolamo Calo [c], Roberto Artali [d], Csaba Tömböly [e], Alicja Kluczyk [f], Anna Janecka [a, *]

[a] Department of Biomolecular Chemistry, Faculty of Medicine, Medical University of Lodz, 92-215, Lodz, Poland
[b] Department of Chemistry, University of Bologna, Via Selmi 2, 40126, Bologna, Italy
[c] Department of Medical Science, Section of Pharmacology and Italian Institute of Neuroscience, University of Ferrara, 44121, Ferrara, Italy
[d] Scientia Advice, di Roberto Artali, 20832, Desio, Monza and Brianza, Italy
[e] Institute of Biochemistry, Biological Research Centre of Hungarian Academy of Sciences, 6701, Szeged, Hungary
[f] Faculty of Chemistry, University of Wroclaw, 50-383, Wroclaw, Poland

ARTICLE INFO

ABSTRACT

Cyclic pentapeptide Tyr-c[D-Lys-Phe-Phe-Asp]NH$_2$, based on the structure of endomorphin-2 (EM-2), which shows high affinity to the μ-opioid receptor (MOR) and a very strong antinociceptive activity in mice was used as a parent compound for the structure–activity relationship studies. In this report we synthesized analogs of a general sequence Dmt-c[D-Lys-Xaa-Yaa-Asp]NH$_2$, with D-1- or D-2-naphthyl-3-alanine (D-1-Nal or D-2-Nal) in positions 3 or 4.

In our earlier papers we have indicated that replacing a phenylalanine residue by the more extended aromatic system of naphthylalanines may result in increased bioactivities of linear analogs. The data obtained here showed that only cyclopeptides modified in position 4 retained the sub-nanomolar MOR and nanomolar κ-opioid receptor (KOR) affinity, similar but not better than that of a parent cyclopeptide. In the in vivo mouse hot-plate test, the most potent analog, Dmt-c[D-Lys-Phe-D-1-Nal-Asp]NH$_2$, exhibited higher than EM-2 but slightly lower than the cyclic parent peptide antinociceptive activity after peripheral (ip) and also central administration (icv). Conformational analyses in a biomimetic environment and molecular docking studies disclosed the structural determinants responsible for the different pharmacological profiles of position 3- versus position 4-modified analogs.

© 2015 Published by Elsevier Masson SAS.

1. Introduction

Seeking new therapies for the treatment of pain is an area of interest for chemists and pharmacologists. Since the endogenous opioid system is known to play a crucial role in pain processing, many endogenous opioid peptides and their synthetic analogs have been studied extensively in order to develop new candidate drugs with antinociceptive activity [1]. There are at least three major types of opioid receptors, μ, δ and κ (or MOR, DOR and KOR, respectively), with distinct profiles clearly distinguishing each one from the others. The scientific breakthrough in opioid receptor research came with obtaining their crystal structures [2–4]. There is evidence that in their inactive form, receptors share a conserved wide-open binding pocket and may function as oligomers [3,5].

According to Yamazaki et al. [6], physiological activity of opioid peptides is determined by the conformation of the N-terminal portion, the so called "message" sequence. The remaining C-terminal fragment represents the "address". This portion is supposed to stabilize the bioactive conformation, among various

conformations accessible to the N-terminal message sequence [7]. As it was well established, Tyr[1] and Phe[3]/Phe[4] residues commonly found in the group of endogenous opioid ligands and their synthetic analogs are structural determinants for binding to opioid receptors [6,8]. Their reciprocal distances and disposition deeply influence the affinity and selectivity for the different opioid receptor subtypes [9,10].

A fundamental step toward the rational design of potent and safe therapeutics is understanding their interactions with receptors which are involved in mediation and modulation of different pharmacological effects. To improve receptor recognition, reduce the molecular conformational freedom, stabilize the peptide in biological fluids and increase membrane permeation, the cyclization of linear sequences was frequently adopted in peptide chemistry [11–14]. The structure of cyclic peptides could be considered a suitable scaffold for arrangement of the pharmacophoric groups in a restricted regions of the space surrounding the molecule [9].

In the search for new, potent antinociceptive agents, we have been synthesizing cyclic analogs based on the structure of endomorphin-2, Tyr-Pro-Phe-PheNH$_2$ (EM-2), with conserved free amino group at the N-terminus which is thought to be crucial for the binding to the MOR [15]. These analogs were cyclized through an amide bond between the side-chains of bifunctional amino acids incorporated into the structure of EM-2 [16–19]. Our first very potent cyclic analog was a pentapeptide Tyr-c[D-Lys-Phe-Phe-Asp] NH$_2$ (analog **1**), which displayed a similar to EM-2 MOR affinity, greatly improved stability in the rat brain homogenate and much stronger and longer lasting antinociceptive activity after intracerebroventricular (icv) administration [16]. This analog elicited analgesia also after peripheral injection and this effect was reversed by the concomitant icv administration of the MOR antagonist, β-funaltrexamine (β-FNA), which indicated that antinociception was mediated by the MOR receptors in the brain. Enzymatic stability and the ability to cross the blood–brain barrier (BBB) are two most desirable features of new analgesic drug candidates which made this cyclic peptide of considerable interest. Therefore, we designed further modifications of this pentapeptide, in order to elucidate structure–activity relationships [17–21]. Continuing these studies, here we report on a new series of cyclic analogs obtained by the introduction of D-1-naphthyl-3-alanine (D-1-Nal) or D-2-naphthyl-3-alanine (D-2-Nal) instead of the Phe residues in positions 3 or 4 of our parent analog **1**. The introduction of a D-amino acid residue into one of these positions in the macrocycle is expected to strongly impact the accessible backbone conformations, since a heterochiral residue tends to stabilize alternative secondary structures. Besides, Nal contains a more extended aromatic ring system and therefore introduces an additional steric hindrance. Additionally, Tyr residue in position 1 was replaced by 2′,6′-dimethyltyrosine (Dmt), known to remarkably enhance opioid receptor binding affinities [22,23]. Introduction of the more lipophilic amino acid residues was aimed at increasing the BBB permeability, while retaining or enhancing the biological activity. The biological properties of the new cyclopeptides were evaluated in the radioligand receptor binding experiments in the rat or guinea pig brain membrane homogenates, followed by determination of their agonist potencies in a calcium mobilization assay performed on cells expressing opioid receptors and chimeric G proteins. The antinociceptive activity of the most promising compound was studied *in vivo* in the mouse hot-plate test. The 3D structure analyses of all new cyclopeptides in solution were performed, and their bioactive conformations when docked into a model of the MOR were obtained. In each test the results were compared to the parent cyclopeptide **1**.

2. Results and discussion

2.1. Synthesis

Peptides were assembled and cyclized on a solid support using a Fmoc/*t*-Bu-based strategy with the hyper-acid labile 4-methyltrityl (Mtt) and 2-phenyl-*iso*propyl ester (O-2 Phi*Pr*) groups [24,25] for the selective amine/carboxyl side-chain protection of D-Lys and Asp, respectively. Analytical properties of the analogs are summarized in Table 1. High resolution mass spectrometry (HR-MS) experiments confirmed the mass identity of all synthesized peptides. RP-HPLC analyses of the final purified products indicated purity of 97% or greater. The structures of the peptides were analyzed by ^{1}H NMR and 2D gCOSY experiments which allowed for the unambiguous assignment of all protons (see Experimental Section).

2.2. Enzymatic stability

The stability of the new cyclopeptides toward enzymatic degradation were verified by measuring their hydrolysis rates in the presence of the rat brain homogenate (Table 1). After 90 min incubation, all cyclopeptides (including parent compound **1**) remained intact in 85–95%, while EM-2 was almost completely digested. The obtained data confirmed that cyclization protects peptides against proteolytic digestion and confers stability in the biological fluids [26]. The cyclic analogs resistant to enzymatic hydrolyses usually exhibit improved bioactivities and bioavailabilities, in comparison with their linear counterparts.

2.3. Receptor binding and functional activity

Opioid receptor binding affinities of new compounds **2**–**5** for the MOR, DOR and KOR were determined by radioligand competition analysis using [3H]DAMGO, [3H][Ile[5,6]]deltorphin-2 and [3H] nor-BNI, respectively. The IC$_{50}$ values were determined from logarithmic dose–displacement curves, and the values of the inhibitory constant (K$_i$) of peptides were calculated according to the equation of Cheng and Prusoff [27].

The K$_i$ values are summarized in Table 2. Analogs **2** and **3** with D-1-Nal or D-2-Nal in position 3, respectively, showed weak affinity for the MOR, did not bind to the DOR and had weak or no affinity for the KOR. Analogs **4** and **5**, similarly modified at position 4, displayed sub-nanomolar MOR affinities compared with the parent compounds, EM-2 and analog **1**. They exhibited also nanomolar KOR affinities, showing weak binding to the DOR (not detectable in case of EM-2).

The pharmacological profiles of analogs **1**–**5** were characterized in calcium mobilization functional assay [19,28,29]. The concentration–response curves of all tested compounds are shown in Fig. 1A–C and the calculated agonist potencies (pEC$_{50}$) and efficacies (α) of the analogs are summarized in Table 3. EM-2, DPDPE, and dynorphin A (Dyn A) were used as the reference full agonists for calculating intrinsic activity at the MOR, DOR and KOR, respectively. In the CHO$_{MOR}$ cells, stably expressing the Gα$_{qi5}$ chimeric protein, compounds **2** and **3** displayed similar potency as the reference MOR agonist (7.70 and 7.94, respectively, compared to 7.88 for EM-2), associated with a significant reduction in efficacy (0.42 ± 0.06 and 0.49 ± 0.03) (Fig. 1A). Cyclopeptides **1**, **4** and **5** mimicked the stimulatory effect of EM-2 (Fig. 1A), displaying a slight reduction of efficacy (0.83 ± 0.09, 0.83 ± 0.05 and 0.75 ± 0.06, respectively) but high potency (8.69, 8.25 and 8.44, respectively).

In the CHO$_{DOR}$ cells, stably expressing the Gα$_{qG66Di5}$ chimeric protein (Fig. 1B), analogs **2** and **3** were completely inactive, while **4** and **5** behaved as partial agonists (0.50 ± 0.05 and 0.31 ± 0.06, respectively) showing potencies (7.19 and 7.27, respectively) not far

Table 1
Physicochemical data and enzymatic stability of the cyclic pentapeptide analogs.

Compd	Sequence	Formula	$m/z[M + H]^{+a}$		RP-HPLC Rt (min)[b]	Area [%][c]
			Calcd	Obsd		
	Tyr-Pro-Phe-Phe-NH$_2$[d] (EM-2)	$C_{32}H_{37}N_5O_5$	571.70	571.85	17.25	0.61 ± 0.04
1	Tyr-c[D-Lys-Phe-Phe-Asp]NH$_2$[d]	$C_{37}H_{45}N_7O_7$	700.345	700.345	20.50	$95.97 \pm 0.70^{***}$
2	Dmt-c[D-Lys-D-1-Nal-Phe-Asp]NH$_2$	$C_{43}H_{51}N_7O_7$	778.392	778.387	16.21	$93.80 \pm 0.50^{***}$
3	Dmt-c[D-Lys-D-2-Nal-Phe-Asp]NH$_2$	$C_{43}H_{51}N_7O_7$	778.392	778.387	16.38	$85.42 \pm 1.00^{***}$
4	Dmt-c[D-Lys-Phe-D-1-Nal-Asp]NH$_2$	$C_{43}H_{51}N_7O_7$	778.392	778.385	16.02	$95.98 \pm 2.02^{***}$
5	Dmt-c[D-Lys-Phe-D-2-Nal-Asp]NH$_2$	$C_{43}H_{51}N_7O_7$	778.392	778.388	16.10	$95.62 \pm 0.81^{***}$

$^{***}p < 0.001$ as compared to EM-2 by using one-way ANOVA followed by the Student—Newman—Keuls test.
[a] Observed by ESI-MS$^+$ ionization.
[b] Rt with Vydac C$_{18}$ column (5 μm, 4.6 × 250 mm) using the solvent system 0.1% TFA in water (A) and 80% acetonitrile in water containing 0.1% TFA (B) and a linear gradient of 0—100% solvent B in 25 min, flow rate 1 mL/min.
[c] Amount of peptide remained after 90 min incubation with rat brain homogenate.
[d] Data from Ref. [16].

Table 2
Opioid receptor binding of the cyclic pentapeptide analogs.

Compd	$K_i{}^a$[nM]		
	MOR	DOR	KOR
EM-2	0.49 ± 0.02	9614.70 ± 834.50	7827.67 ± 948.20
1	0.35 ± 0.02	170.86 ± 3.5	1.12 ± 0.20
2	69.18 ± 1.20	9173.80 ± 920.60	56.62 ± 2.50
3	16.82 ± 0.60	4248.85 ± 566.50	750.70 ± 4.10
4	0.25 ± 0.02	51.20 ± 3.00	1.78 ± 0.15
5	0.44 ± 0.03	110.35 ± 8.10	1.02 ± 0.40

[a] Binding affinities are given as K_i values determined by competitive displacement of the selective radioligands, [^{3}H]DAMGO or [^{3}H][Ile^{5,6}]deltorphin-2 using rat brain membranes, and [^{3}H]nor-BNI using guinea pig brain membranes. All values are expressed as mean $\pm$ SEM of three independent experiments performed in duplicate.

2.4. Antinociceptive activity

The antinociceptive effect of analogs was assessed in the mouse hot-plate test which evaluates central pain attenuation after applying an acute thermal stimuli and was compared to the effect produced by EM-2. Groups of mice were injected icv and the hot-plate responses were measured 10 min after injection. The results obtained after the icv administration of peptides showed that analogs **2** and **3** (ED$_{50}$ for jumping 0.714 and 0.533 μg/animal, respectively) produced responses slightly better than EM-2 (ED$_{50}$ for jumping 1.820 μg/animal) despite their lower MOR affinity, what could be explained by much higher enzymatic stability of the cyclopeptides. The strongest antinociceptive effect, similar to that of the parent peptide **1**, was produced by **4** and **5** (ED$_{50}$ for jumping
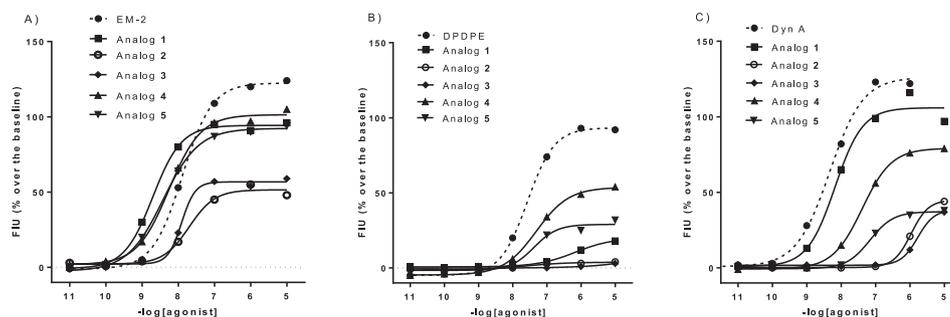

Fig. 1. Concentration response curves for the cyclic pentapeptide analogs **1**—**5** and EM-2 (A), DPDPE (B) and Dyn A (C) in calcium mobilization experiments performed in A) CHO$_{MOR}$, B) CHO$_{DOR}$ and C) CHO$_{KOR}$ cells, respectively.

from that of DPDPE (7.57) (Fig. 1B), while the curve for analog **1** was incomplete.

Finally, in the CHO$_{KOR}$ cells stably expressing the Gα$_{qi5}$ chimeric protein, compound **1** mimicked the stimulatory effect of Dyn A, showing high potency (8.18) and maximal effect (106 ± 9%). Compound **4** exhibited also relatively high potency (7.38), associated however with a significant reduction of maximal effect (79 ± 6%). Peptides **2**, **3** and **5** exhibited lower potency (5.77—6.99) and efficacy (Fig. 1C).

Summing up, the parent peptide **1** was a mixed MOR/KOR full agonist, with similar potency at both these receptors. Analogs **4** and **5** also behaved as mixed MOR/KOR agonists but showed significantly higher potency and efficacy at the MOR, being therefore more selective than **1**. Compounds **2** and **3** were partial MOR agonists with moderate selectivity for this receptor.

0.05, 0.06 and 0.08 μg/animal, respectively) (Fig. 2) which was well correlated with their sub-nanomolar MOR and nanomolar KOR affinity.

The results of the hot-plate test after ip administration of peptides are shown in Fig. 3. Groups of mice were injected the cyclopeptides ip in a dose range of 0.1—10 mg/kg (except analogs **2** and **3** which were injected only in two higher doses) and the hot-plate responses were measured 15 min after injection. Analogs **1**, **4** and **5** (ED$_{50}$ for jumping <0.01, 1.160 and 3.244 mg/kg, respectively) showed significant, dose-dependent antinociceptive activity (88, 82 and 55% at 10 mg/kg, respectively), while for **2** and **3** much weaker effects were observed only at the highest dose (17 and 24%, respectively).
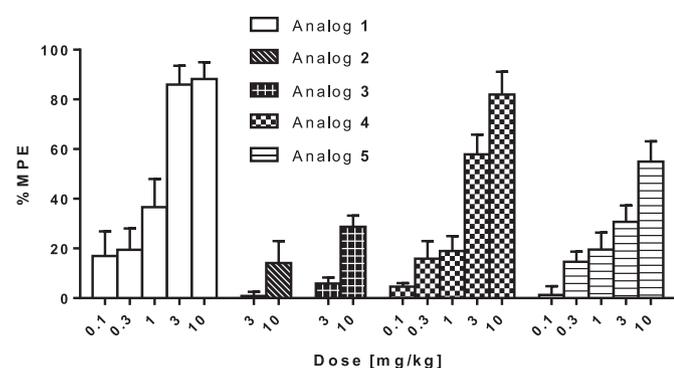
The time-course experiments were performed following the ip administration of two best analogs **4** and **5** at a dose of 3 mg/kg and compared with **1** (Fig. 4). The hot-plate responses were measured
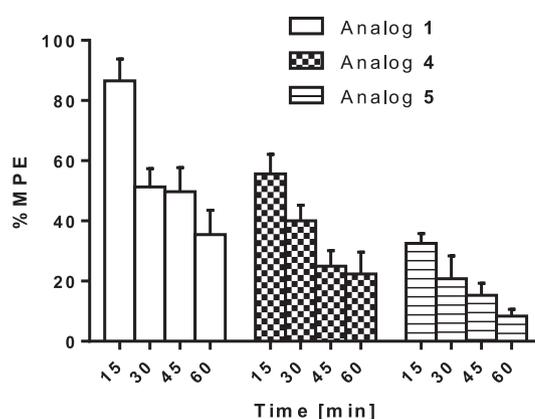
Table 3
Effects of novel cyclic pentapeptide analogs at human recombinant opioid receptors coupled with calcium signaling *via* chimeric G proteins.

Compd	MOR		DOR		KOR	
	pEC$_{50}$[a] (CL$_{95\%}$)	$\alpha \pm$ SEM[b]	pEC$_{50}$ (CL$_{95\%}$)	$\alpha \pm$ SEM	pEC$_{50}$ (CL$_{95\%}$)	$\alpha \pm$ SEM
DPDPE	Inactive[c]		7.57 (7.41—7.73)	1.00	Inactive[c]	
Dyn A	6.67[d] (6.17—7.17)	0.83 $\pm$ 0.10[d]	7.73 (7.46—8.00)	0.99 $\pm$ 0.04[d]	8.35 (8.16—8.53)	1.00
EM-2	7.88 (7.72—8.05)	1.00	Inactive[c]		Inactive[c]	
1	8.69 (8.10—9.29)	0.83 $\pm$ 0.09	Crc incomplete		8.18 (8.01—8.36)	1.00 $\pm$ 0.01
2	7.70 (7.46—7.94)	0.42 $\pm$ 0.06*	Inactive[c]		5.89 (5.62—6.17)	0.43 $\pm$ 0.05*
3	7.94 (7.64—8.24)	0.49 $\pm$ 0.03*	Inactive[c]		5.77 (5.44—6.09)	0.31 $\pm$ 0.04*
4	8.25 (8.08—8.43)	0.83 $\pm$ 0.05	7.19 (6.89—7.49)	0.50 $\pm$ 0.05*	7.38 (7.24—7.52)	0.74 $\pm$ 0.06*
5	8.44 (8.20—8.69)	0.75 $\pm$ 0.06*	7.27 (6.87—7.68)	0.31 $\pm$ 0.06*	6.99 (6.71—7.27)	0.44 $\pm$ 0.04*

EM-2, DPDPE and Dyn A were used as reference agonists for calculating intrinsic activity at the MOR, DOR, and KOR, respectively.
*$p < 0.05$ according to one way ANOVA followed by the Dunnett test for multiple comparisons.
[a] Agonist potency values (pEC$_{50}$) and.
[b] Efficacy values (α).
[c] Inactive means that the compound was inactive as agonist up to 1 μM.
[d] Data from Ref. [28]. The data represent mean $\pm$ SEM of at least 3 separate experiments performed in duplicate.
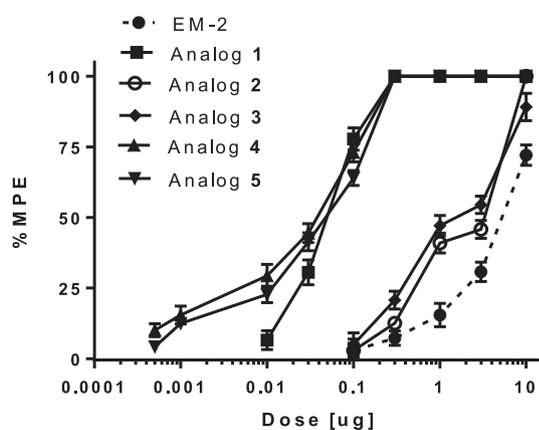
Fig. 2. The effect of different doses of the cyclic pentapeptide analogs **1**—**5** and EM-2 in the mouse hot-plate test. Results are expressed as percentage (mean $\pm$ SEM) of the maximal possible effect (%MPE) for the inhibition of jumping induced by icv injection of a peptide. Number of animals per group ranged between 7 and 10.

Fig. 4. Antinociceptive effect of **1**, **4** and **5** (3 mg/kg) in the mouse hot-plate test at different times after ip injection. Results are expressed as percentage (mean $\pm$ SEM) of the %MPE for the inhibition of jumping. Number of animals per group ranged between 7 and 10.

Fig. 3. The effect of different doses of the cyclic pentapeptide analogs **1**—**5** in the mouse hot-plate test. Results are expressed as percentage (mean $\pm$ SEM) of the %MPE for the inhibition of jumping induced by ip injection of a peptide. Number of animals per group ranged between 7 and 10.

15, 30, 45, and 60 min after injection. The strongest antinociceptive effects were observed 15 min after injection, then slowly declined.

Two of the new lactams (**4** and **5**) showed, similarly to parent compound **1**, efficacy to both, MOR and KOR. Compounds which display strong antinociception after peripheral administration and bind simultaneously to MOR and KOR may represent a new

generation of pain relieving peptides with reduced abuse liability. Central action of KOR agonists produces analgesia accompanied by some dysphoric effects [30,31], and that property has limited the therapeutic development of this class of ligands [32,33]. However, some evidence suggests that mixed MOR/KOR agonists display fewer side-effects. Indeed, MOR/KOR agonists of alkaloid structure, such as ethylketazocine (EKC), have been known and used to treat cocaine addiction [31,34]. Presumably, the presence of MOR agonist activity can neutralize any dysphoria induced by KOR agonism [31,35].

2.5. Conformational analysis

The different activity profiles of the cyclopeptides prompted us to investigate the preferred conformations of the new analogs **2**—**5** in solution by ^{1}H NMR spectroscopy and restrained molecular dynamics (MD), as previously reported [36]. NMR spectra were recorded in 8:2 mixtures of deuterated dimethyl sulfoxide (DMSO-d_6) and H$_2$O. Such mixed solvent system have been recommended by several authors as an excellent representative of biological fluids [37,38]. All the spectra showed a single set of resonances, suggestive of conformational homogeneity or a rapid equilibrium between conformers. It is apparent that peptides **2** and **3**, containing D-Nal at position 3, had very similar spectra, with the diverse resonances at nearly the same chemical shift values. In a similar way, peptides **4**

and **5** containing D-Nal at position 4, displayed very similar ^{1}H NMR spectra (see Experimental Section, NMR analysis section).

Variable-temperature (VT) ^{1}H NMR experiments performed in 8:2 mixture of DMSO-d_6/H$_2$O were used to detect if amide protons were involved in the intramolecular hydrogen bonding or were solvent exposed (Table 4). Cyclopeptides **2** and **3** showed comparatively lower $\Delta\delta/\Delta T$ values for Asp[5]NH in respect to other amide protons ($\Delta\delta/\Delta T$ in p.p.b./K, for **2** = −2.4, for **3** = −2.6), suggestive of some preference for conformations having hydrogen bonded AspNH ($|\Delta\delta/\Delta T| \leq 2.5$ p.p.b./K) [39]. On the other hand, the cyclopeptides **4** and **5** showed a low $\Delta\delta/\Delta T$ value for D-Phe[3]NH ($\Delta\delta/\Delta T = -1.6$ p.p.b./K) but the $\Delta\delta/\Delta T$ values for the remaining amide protons of the macrocycle were only slightly higher, ranging from −2.5 to 3.6 p.p.b./K, thus suggesting that these peptide might adopt a variety of conformations characterized by weak hydrogen bonds.

Detailed conformational analyses of cyclopeptides **2**–**5** were performed by 2D NMR spectroscopy and MD simulations. The compounds were analyzed by 2D-ROESY in the biomimetic DMSO-d_6/H$_2$O (8:2) mixed solvent. Cross-peak intensities were ranked to inter plausible inter-proton distances as restraints (Supplementary Material). Structures consistent with ROESY were obtained by simulated annealing with restrained MD in a box of explicit TIP3P equilibrated water molecules. The ω bonds were set at 180°; as it is well established that peptides comprising only secondary amide bonds adopt all-*trans* conformations. In any case, the absence of Hα(*i*)−Hα(*i* + 1) cross-peaks reasonably excluded the occurrence of *cis* peptide bonds. The structures were minimized with the AMBER force field [40] and clustered by the rmsd analysis of backbone atoms.

For analog **2**, the procedure gave one major cluster comprising the large majority of the structures. The representative structure with the lowest energy was selected and analyzed (Fig. 5). In the ROESY-derived structure, the Dmt residue was situated above the plane of the macrocycle (Fig. 5). The backbone adopted an inverse type II β-turn secondary structure centered on D-1-Nal-Phe, stabilized by a hydrogen bond between D-Lys carbonyl oxygen and AspNH, in agreement with the VT-NMR experiments (Table 4). On the other hand, **2** showed also a hydrogen bond between D-LysNH and Asp C = O, not predicted by VT-NMR analysis; possibly this hydrogen bond was not as stable as the previous one, due to the floppy geometry of the long Lys side chain connecting Asp.

On repeating the procedure described above, analog **3** gave a single major cluster of conformers, whose representative, lower energy model was characterized by a type I β-turn secondary structure centered on D-2-Nal-Phe, with a hydrogen bond between D-Lys carbonyl oxygen and AspNH (Fig. 5). Possibly, the presence of the 2-Nal substituent instead of the 1-Nal isomer at position 3 of the macrocycle forced the phenyl side chain of Phe[4] above the molecular plane, so adopting a pseudo axial disposition, impacting also the geometry of the flexible Lys (CH$_2$)$_4$ chain.

The analysis of analog **4** gave one major cluster showing the Dmt residue in a pseudo equatorial position in respect to the macrocycle, and a second minor cluster in which Dmt was located above the plane of the macrocycle. The respective structures **4A** and **4B**, with

the lowest energies (**4A** comparatively more stable than **4B**) were selected and analyzed (Fig. 5). Both conformations were characterized by a type II β-turn centered on Phe-D-1-Nal with a hydrogen bond between D-LysNH and AspC = O. Nevertheless, the VT-NMR analysis indicated that other hydrogen bonded structures involving either D-LysNH and/or PheNH were possible (Table 4). Reasonably, **4A** and **4B** represented conformers in equilibrium, whose average accounted for the medium ROESY cross-peak between PheNH and D-LysHα (corresponding to a distance of about 3 Å). These correlations and the secondary structures of **2**, **3**, **4A**, **4B**, and **5** along with the explicit hydrogen bonds, are also sketched in Fig. 8 (Discussion Section).

Finally, the investigation of the conformational features of analog **5** by 2D ROESY and MD gave, after clustering, a single model structure very similar to **4A** (Fig. 5). Accordingly, **5** showed a clear hydrogen bonded type II β-turn centered on Phe-D-2-Nal. Unlike in case of **2** and **3**, the substitution of 1-Nal with 2-Nal did not prevent **5** from adopting the same backbone geometry as **4A**, indicating that also the stereochemistry array of the residues (LDDLL for **2** and **3**, LDLDL for **4** and **5**) exerted a significant role in determining the overall 3D structure [41,42].

The structures of **2**–**5** determined in solution (Fig. 5) were compared to the in-solution conformations of the parent peptide **1** described earlier [20]. The analysis of the conformations of backbones and side-chains revealed that the Tyr-D-Lys-Phe portions of **4A** and **5** maintained a good superimposition with the corresponding portions of analog **1** sol. However, **4A** and **5** differ in the positioning of the naphthyl groups and in the conformation of Asp, correlated to the reversal of configuration of the fourth residue. On the other hand, the structures of **2** and **3** carrying the D-configured residue at position 3 clearly differ from the structure of analog **1** sol. both in terms of backbones and all side-chain orientations.

2.6. Molecular docking

All compounds were analyzed by molecular docking (MolDock) simulations with Autodock 4.0 [43], using as initial geometries of the ligands the ROESY-derived structures shown in Fig. 5, and the previously reported model of human MOR (hMOR) obtained by homology modeling [41,44,45], subsequently validated using the crystallographic structure obtained in 2012 [2]. The results from this procedure were followed by relaxation and optimization of the resulting system (induced-fit). A combined quantum mechanical/molecular mechanics (QM/MM) approach was utilized to study the ligand-receptor complex [41,45]. In this method, an accurate but computationally intensive QM description was used only for regions where electronic interactions were occurring. The rest of the system, whose chemical identity remained essentially the same, was treated at the approximate classical MM level. Structures were clustered together and representative model of each cluster was selected based on the most favourable free energy of binding.

The compounds **4** and **5** differed only by the side-chain of the residue present at position 4, D-1-Nal or D-2-Nal, respectively. Regardless of this difference, both compounds were able to interact effectively with the binding site, providing two complexes perfectly inserted into the cavity and showing the well-known ionic interaction between the quaternary cationic nitrogen of Dmt and the Asp147 (TMH III). This interaction was enhanced by a second hydrogen bond with the Tyr326 (EL IV) (Fig. 6A and B for **4** and **5**, respectively). The AspCONH$_2$ group of both ligands was situated in a zone adjacent to EL II and TMH V. In this position it was able to effectively interact with the residue Glu229 (TMH V). The aliphatic and aromatic portions of the ligands were positioned in close proximity to the hydrophobic pockets belonging to domains TMH I, TMH II, TMH III and TMH VII, with the naphthalene group able to

Table 4
$\Delta\delta/\Delta T$ values (p.p.b./K) for the amide protons of the cyclic pentapeptide analogs **2**–**5** in 8:2 DMSO-d_6/H$_2$O.

Compd	D-Lys[2]NH	Xaa[3]NH	Yaa[4]NH	Asp[5]NH	D-LysNHε	CONH$_2$
2	−4.3	−3.3	−8.2	−2.4	−3.6	−5.7/−6.2
3	−4.6	−4.1	−6.1	−2.6	−3.9	−4.5/−4.5
4	−2.5	−1.6	−3.6	−2.5	−3.5?	−4.5/−4.7
5	−2.5	−1.6	−3.2	−2.9	−3.1	−4.7/−4.7

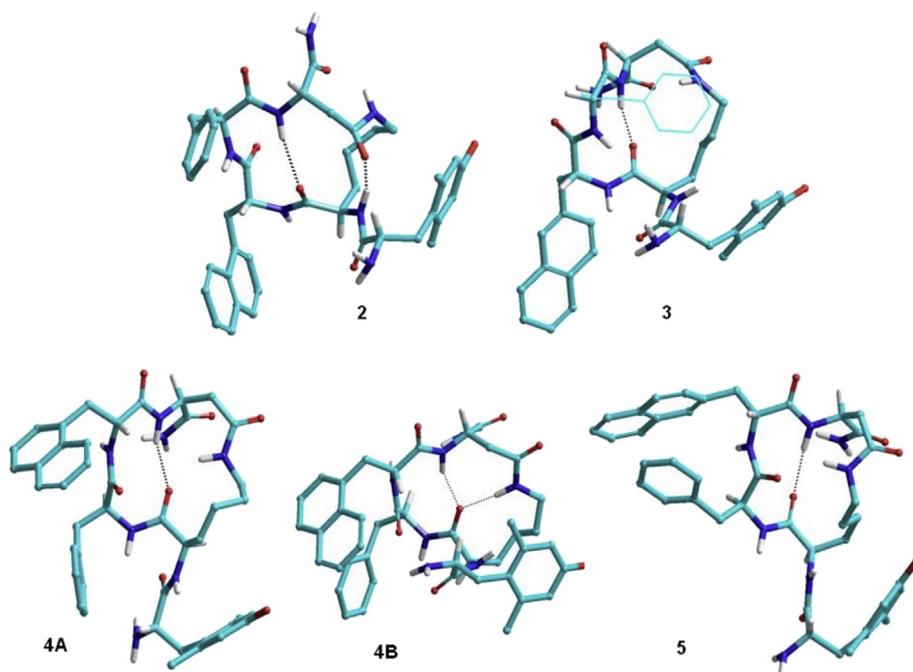**Fig. 5.** Representative lowest energy structures of **2**–**5**, calculated by ROESY-restrained MD in a 30 × 30 × 30 Å box of standard TIP3P water molecules. Only amide and α-protons are shown.
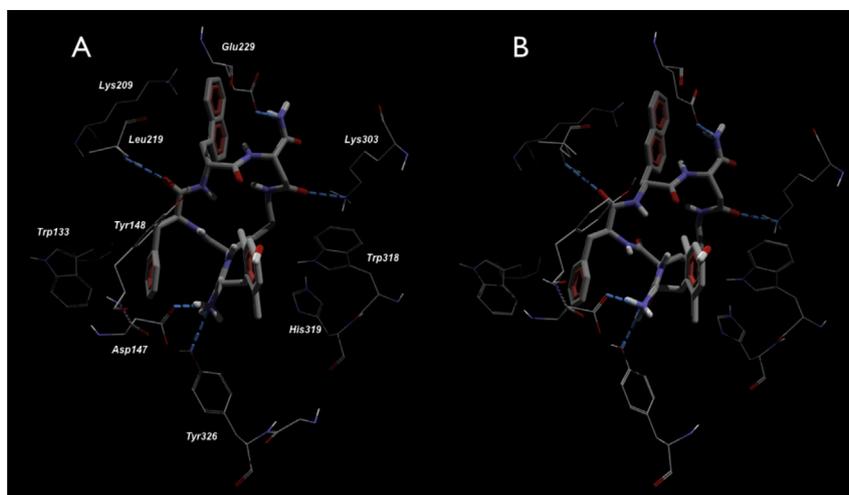

Fig. 6. The schematic 3D diagrams of the interactions between analog **4** (A) and analog **5** (B) with hMOR, and amino acid composition of the binding site. Residues belonging to the hMOR are shown in wire frame, while the ligands are in sticks. Hydrogen bonds are represented by dashed lines.

interact with Lys209 (EL III) *via* a cation–pi interaction. The interaction pattern was completed by two hydrogen bonds with Lys303 (TMH VI) and Leu219 (EL III). The structural similarities described above were confirmed by the very similar values of the free energies of binding, with **4** being only 0.9 kcal/mol more stable than **5**. The schematic 3D diagrams of the interactions between the ligands and hMOR are shown in Fig. 6A and B, along with the amino acid composition of the binding site.

The MolDock computations of analogs **2** and **3** confirmed also for these compounds the occurrence of the ionic interaction with Asp147 (TMH III), while the carbonyl group of Dmt residue interacted with Tyr148 (TMH III). Compound **3** (Fig. 7B) showed two additional hydrogen bonds with Glu229 (TMH V) and Ile296 (TMH VI) which were not found in compound **2** (Fig. 7A). Both

compounds displayed a pi–pi interaction between the naphthyl group of Nal[3] and Tyr128 (TMH II). However, in this position, the naphthyl group was affected by a strong steric hindrance, resulting in less stable complexes compared to **4** and **5**. A measure of this instability was given by the difference in the calculated binding free energy of **2** and **3** compared to the value obtained for **4**, amounting to 12.7 and 10.3 kcal/mol, respectively. The schematic 3D diagrams of the ligand-receptor interactions and the amino acid composition of the binding site, are shown in Fig. 7.

Compared to the bioactive conformation of the parent compound **1**, **4** and **5** adopt within the receptor the same geometry of Tyr-D-Lys-Phe, while the portions D-Nal-Asp are significantly different. The reversal of stereochemistry of D-Nal[4] with respect to L-Phe[4] of the parent peptide **1** drives the large naphthyl side-chain
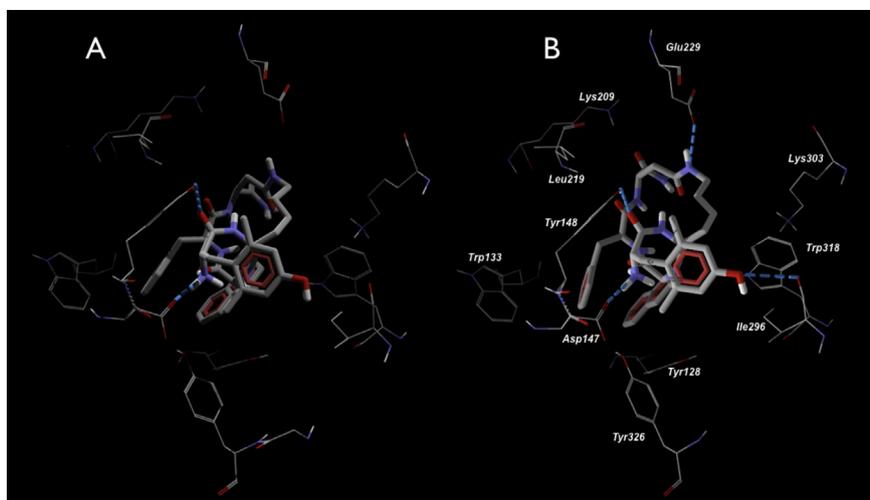
Fig. 7. The schematic 3D diagrams of the interactions between analog **2** (A) and analog **3** (B) with hMOR, and residue composition of the binding site. Residues belonging to the hMOR receptor are shown in wire frame, while the ligands are in sticks. Hydrogen bonds are represented by dashed lines.
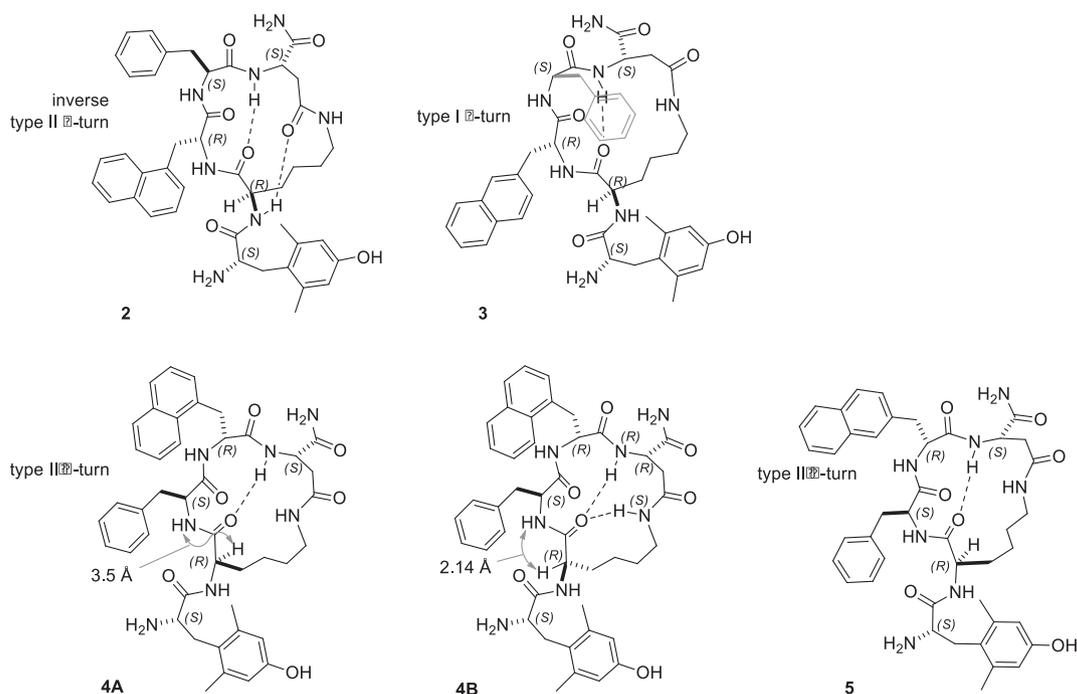

Fig. 8. Sketches of the structures of **2**–**5** (to be compared to Fig. 5).

to occupy an alternative position. Nevertheless, the docking structures reported in Fig. 6 show that the naphthyl group of **4** and **5** can be easily hosted in an upper hydrophobic cavity delimited by the residues Glu229, Lys209, Leu219, so the compounds can still efficiently fit the receptor. Interestingly, the substitution of L-Phe[4] by D-Nal[4] also induces a rotation of the analogs **4** and **5** within the receptor cavity with respect to the parent analog **1**. Indeed, while the latter interacts with Tyr[148] of the protein by a hydrogen-bond with Tyr[1](C=O), in **4** and **5** the phenyl of Phe[3] is situated side-by-side with Tyr[148] (Fig. 6).

As for the derivatives **2** and **3**, the comparison of the bioactive structures with that of the parent analog **1** shows a completely different binding poses (Fig. 7). Possibly, the very large side-chains of D-Nal[3] cannot easily accommodate into the small pocket

delimited by residues Asp147, Tyr148, Trp133, so the entire structure is forced to enter in a lying down position, to minimize unfavorable clashes.

In summary, the biological activities of the peptides **2**–**5** can be correlated with the different structural features. The very similar ^{1}H NMR spectra and VT-NMR experiments for **2** and **3** and also for **4** and **5** indicate that cyclopeptide backbone conformations were scarcely influenced by the different structures of the side-chains (1-Nal *versus* 2-Nal). As a matter of fact, the 2D ROESY-derived structures of **2** and **3** showed a somewhat different display of the aryl side-chains of D-Nal[3] and Phe[4], and minor differences relative to the highly flexible $(CH_2)_4$ connector between Lys and Asp. For compound **4**, the conformational analysis gave two possible conformers, characterized by a rather different position of the

fundamental residue Dmt[1]. On the other hand, the predominant conformer **4A** was very similar to the conformation of compound **5**. The comparison of all structures (Fig. 8) revealed that the Dmt[1] residue adopted in all cases the same position, nearly equatorial to the macrocycle. Therefore, the most striking difference between **2/3** and **4/5** seems to be a different display of the side-chains of the residues at the positions 3 and 4, mostly correlated to the different stereochemistry array, LDDLL for **2** and **3**, *versus* LDLDL for **4** and **5**.

This major difference resulted in a different ability to fit the opioid receptor. The MolDock analyses showed the binding poses of the cyclopeptides and the residues involved in the ligand-receptor recognition. The computations revealed that the most relevant differences between **2/3** and **4/5** involved the naphthyl groups. Compared to the binding poses of **4/5**, the shift of the naphthyl groups from position 4 to position 3 had the effect of preventing the cation−pi interaction between the naphthyl group and Lys209 (EL III), fostering instead a pi−pi interaction with Tyr128 (TMH II). However, in this position, the naphthyl group of **2/3** (Fig. 7) was affected by a strong steric hindrance, resulting in less stable complexes as compared to **4/5**. Interestingly, it turned out that bioactive conformations of **2−5** are slightly different from that of the parent analog **1**. In particular, the inspection of Fig. 6 showed that, unlike **1**, these cyclopeptides reproduce most of the fundamental interactions of the prototypic potent MOR-selective agonist JOM-6 (Fig. 9) [44,46].

3. Conclusion

Performing the structure−activity relationship studies of our cyclic pentapeptide Tyr-c[D-Lys-Phe-Phe-Asp]NH$_2$ (**1**), which showed a very strong antinociceptive activity in mice after central and peripheral administration we obtained a series of lactams, incorporating D-1- or D-2-Nal residues in positions 3 or 4. Analogs modified in position 4 showed significantly higher opioid receptor affinities and pharmacological activities than the position-3 substituted counterparts. On the other hand, substitution of D-1-Nal *versus* D-2-Nal in each of the two positions produced similar results. Pharmacological assays revealed that peptides **2** and **3,** having D-Nal in position 3, behaved as weak MOR and KOR

agonists. Peptides **4** and **5** with D-configured 1-Nal or 2-Nal in position 4, were similarly to the parent compound **1**, excellent ligands of MOR with sub-nanomolar affinity and good KOR ligands with nanomolar affinity. In the calcium mobilization functional test, these two peptides were found to behave as universal opioid receptor agonists, with markedly higher potency and efficacy for the MOR. In agreement with high MOR affinity and partial agonism, **4** and **5** displayed high antinociceptive activity in mice when delivered by icv but also ip injection. As compared with analog **1**, compounds **4** and **5** showed slightly higher antinociception after icv administration but slightly lower after systemic (ip) administration. The conformational analyses in solution and the MolDock computations suggested that the different ligand-receptor recognition of the pairs **2/3** and **4/5** can be correlated to the different position and 3D display of the bulky naphthyl groups. On the other hand, the bioactive conformations adopted within the receptor by peptides **1** and **4/5** showed similar binding poses which probably determined their alike pharmacological properties.

4. Experimental section

4.1. Materials and methods

All reagents, unless otherwise stated, were purchased from Sigma Aldrich (Poznan, Poland). Protected amino acids were purchased from Bachem AG (Bubendorf, Switzerland). Opioid radioligands, [³H]DAMGO, [³H][Ile⁵,⁶]deltorphin-2 and [³H]nor-BNI were obtained from Biological Research Centre of Hungarian Academy of Sciences (Szeged, Hungary). Analytical and semi-preparative RP-HPLC was performed using Waters Breeze instrument (Milford, MA, USA) with dual absorbance detector (Waters 2487) on Vydac C$_{18}$ column (5 μm, 4.6 × 250 mm) and Vydac C$_{18}$ column (10 μm, 22 × 250 mm), respectively. Mass spectra of peptides (Supporting Information) were recorded on FT-ICR (Fourier transform ion cyclotron resonance) Apex-Qe Ultra 7T instrument (Bruker Daltonics, Bremen, Germany). ¹H NMR spectra of peptides were recorded at 400 MHz in 8:2 DMSO-d_6/H$_2$O at room temperature.

4.2. Solid-phase peptide synthesis

All peptides were synthesized as previously described by Perlikowska et al. [18], using techniques for Fmoc-protected amino acids on MBHA Rink-Amide peptide resin (100−200 mesh, 0.8 mmol/g). N^ε-amino group of D-Lys was protected by Mtt, β-carboxy group of Asp by O-2 PhiPr and hydroxy group of Dmt by *t*-butyl (*t*-Bu). Completion of coupling reactions was monitored by the chloranil test [47]. Crude peptides were purified by semi-preparative RP-HPLC using Waters Breeze instrument (Milford, MA, USA). The correctness of the syntheses was confirmed by HR-MS.

4.3. Opioid receptor binding assays

Opioid receptor binding assays were performed according to the method described in detail elsewhere [16], using brain homogenates of adult male Wistar rats (for MOR and DOR) or adult male Dunkin Hartley guinea pigs (for KOR). Binding affinities of peptides for MOR, DOR and KOR were measured against tritiated radioligands, [³H]DAMGO, [³H][Ile⁵,⁶]deltorphin-2 and [³H]nor-BNI, respectively. The data were analyzed by a nonlinear least square regression analysis computer program Graph Pad PRISM 6.0 (GraphPad Software Inc., San Diego, USA).
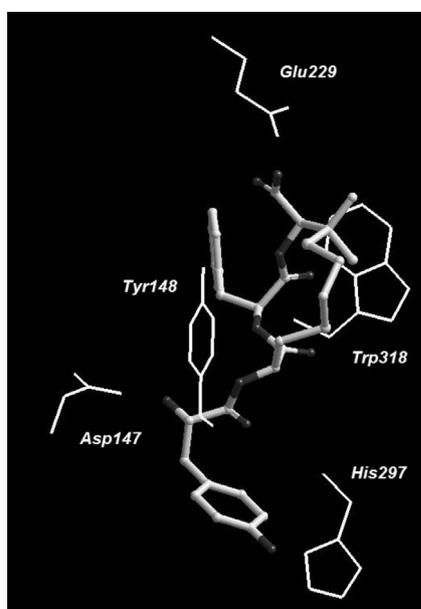

Fig. 9. A sketch of the MOR-binding pose of JOM-6 (in ball and cylinders), and relevant interactions with receptor residues (in sticks) (to be compared to Fig. 6).

4.4. Metabolic stability

Enzymatic degradation studies of the new analogs were performed using Wistar rat brain homogenate, following the method reported in detail previously [16]. Briefly, the analogs were incubated with brain homogenate over 0, 7.5, 15, 22.5, 30 and 90 min at 37 °C. The reaction was monitored by RP-HPLC and the amount of the remaining peptide (area %) was assessed.

4.5. Calcium mobilization assay

CHO cells stably co-expressing human recombinant KOR or MOR and the C-terminally modified $G\alpha_{qi5}$ [48], and CHO cells co-expressing the human recombinant DOR and the $G\alpha_{qG66Di5}$ chimeric protein [49], were generated and used in mobilization assay as previously described [19,28].

Agonist potencies were given as pEC_{50} representing a negative logarithm of the molar concentration of an agonist that produces 50% of the maximal possible effect. Concentration response curves were fitted with the four parameter logistic nonlinear regression model:

$$Effect = baseline + \frac{E_{max} - baseline}{1 + 10^{(logEC_{50}-X)\cdot n}}$$

where X is the agonist concentration and n is the Hill coefficient. Ligand efficacy was expressed as intrinsic activity (α) calculated as the E_{max} of the ligand to E_{max} of the standard agonist ratio. Curve fittings were performed using GraphPad PRISM 6.0 (GraphPad Software Inc., San Diego, USA).

4.6. Assessment of antinociception

The procedures used in this study were in accordance with the European Communities Council Directive (86/609/EEC), and approved by the Local Ethical Committee for Animal Research at the Medical University of Lodz with the following number: 29/ŁB 662/2013.

Male albino mice (BalbC, Animal House, Faculty of Pharmacy, Lodz, Poland), weighing 20–26 g, were used throughout the study. The animals were housed under controlled environmental conditions (temperature: 22 ± 1 °C, 7 am to 7 pm light–dark cycle) with free access to standard semi-synthetic laboratory diet and tap water *ad libitum*. Mice were tested only once and sacrificed immediately thereafter by decapitation.

The antinociceptive effects of peptides were assessed in the hot-plate test, according to the method of Eddy and Leimbach [50] and adapted in our laboratory by Fichna et al. [17]. The icv injections (10 μL/animal) of peptides or a vehicle were performed in the left brain ventricle of manually immobilized mice with a Hamilton micro-syringe (50 μL) connected to a needle (diameter 0.5 mm) while ip injections (100 μL/animal) were performed into the peritoneum. The latencies to jumping were measured.

A transparent plastic cylinder (14 cm diameter, 20 cm height) was used to confine a mouse on the heated (55 ± 0.5 °C) surface of the plate. The animals were placed on the hot-plate 10 min after icv injection or 15 min after ip injection. A cut-off time of 240 s was used to avoid tissue injury.

The percentage of the maximal possible effect (%MPE) was calculated as: $\%MPE = (t_1-t_0)/(t_2-t_0) \times 100$, where t_0 — control latency, t_1-test latency and t_2 — cut-off time (240 s). The median antinociceptive dose (ED_{50}) was calculated as described earlier [16]. The data were analyzed by a nonlinear least square regression analysis computer program Graph Pad PRISM 6.0 (GraphPad Software Inc., San Diego, USA).

4.7. NMR analysis

^1H NMR spectra were recorded with a Varian Gemini apparatus at 400 MHz in 5 mm tubes, using 0.01 M peptide at room temperature (Supporting Information). Solvent suppression was performed by the solvent presaturation procedure implemented in Varian (PRESAT). Chemical shifts were reported as δ values relative to residual DMSO (δ_H = 2.50 ppm) as internal standard. The unambiguous assignment of ^1H NMR resonances was based on 2D gCOSY experiments. VT-^1H NMR experiments were performed over the range of 298–348 K; temperature calibration was done with the ethylene glycol OH−CH chemical-shift separation method.

Dmt-c[D-Lys-D-1-Nal-Phe-Asp]NH$_2$ (**2**). ^1H NMR (400 MHz, 8:2 DMSO-d_6/H$_2$O) δ: 0.41 (m, 1H, LysHγ), 0.66 (m, 1H, LysHγ), 1.02 (m, 1H, LysHδ), 1.10−1.20 (m, 2H, LysHδ + LysHβ), 1.42 (m, 1H, LysHβ), 2.13 (s, 6H, DmtMe), 2.32 (dd, J = 3.0, 13.0 Hz, 1H, AspHβ), 2.55 (dd, J = 8.2, 13.0 Hz, 1H, AspHβ), 2.68−2.75 (m, 2H, DmtHβ + NalHβ), 2.76−2.82 (m, 2H, PheHβ + LysHε), 2.83−2.98 (m, 4H, DmtHβ + NalHβ + PheHβ + LysHε), 3.97 (m, 1H, DmtHα), 4.27 (m, 1H, LysHα), 4.40 (ddd, J = 3.0, 8.0, 8.2 Hz, 1H, AspHα), 4.62−4.72 (m, 2H, PheHα + NalHα), 6.34 (s, 2H, DmtArH$_{3,5}$), 7.08−7.20 (m, 5H, PheArH + CONH$_2$), 7.22−7.26 (m, 2H, PheArH), 7.34 (m, 1H, NalArH$_3$), 7.39 (t, J = 6.0 Hz, 1H, LysNHε), 7.51 (t, J = 7.2 Hz, 1H, NalArH$_6$), 7.57 (t, J = 7.2 Hz, 1H, NalArH$_7$), 7.75 (brd, 1H, NalH$_4$), 7.89 (d, J = 8.4 Hz, 1H, NalArH$_5$), 7.90 (d, J = 9.2 Hz, 1H, LysNH), 8.02 (d, J = 8.0 Hz, 1H, AspNH), 8.12−8.22 (m, 3H, DmtNH + NalArH$_8$), 8.28 (d, J = 8.8 Hz, 1H, NalNH), 8.66 (d, J = 8.8 Hz, PheNH), 9.01 (s, 1H, DmtOH).

Dmt-c[D-Lys-D-2-Nal-Phe-Asp]NH$_2$ (**3**). ^1H NMR (400 MHz, 8:2 DMSO-d_6/H$_2$O) δ: 0.40 (m, 1H, LysHγ), 0.65 (m, 1H, LysHγ), 1.00 (m, 1H, LysHδ), 1.12−1.20 (m, 2H, LysHβ + LysHδ), 1.42 (m, 1H, LysHβ), 2.13 (s, 6H, DmtMe), 2.32 (dd, J = 3.6, 15.2 Hz, 1H, AspHβ), 2.52−2.60 (m, 2H, NalHβ + AspHβ), 2.63 (dd, J = 4.0, 14.0 Hz, 1H, NalHβ), 2.69−2.80 (m, 2H, PheHβ + DmtHβ), 2.85 (m, 1H, LysHε), 2.89−3.00 (m, 3H, DmtHβ + PheHβ + LysHε), 3.96 (m, 1H, DmtHα), 4.32 (m, 1H, LysHα), 4.38 (ddd, J = 3.6, 4.8, 8.0 Hz, 1H, AspHα), 4.60 (ddd, J = 4.0, 6.0, 9.6 Hz, 1H, PheHα), 4.65 (ddd, J = 4.0, 7.2, 8.8 Hz, 1H, NalHα), 6.34 (s, 2H, DmtArH$_{3,5}$), 7.06 (s, 1H, CONH$_2$), 7.12−7.19 (m, 4H, CONH$_2$ + PheArH), 7.20−7.24 (m, 2H, PheArH), 7.27 (d, J = 8.0 Hz, NalArH$_3$), 7.32 (t, J = 6.0 Hz, 1H, LysNHε), 7.42−7.49 (m, 2H, NalArH$_{6,7}$), 7.60 (s, 1H, NalArH$_1$), 7.76 (d, J = 8.0 Hz, 1H, NalArH$_4$), 7.83 (d, J = 8.0 Hz, 1H, NalArH$_5$), 7.90 (d, J = 7.6 Hz, 1H, LysNH), 8.01 (d, J = 8.0 Hz, 1H, AspNH), 8.11 (br.s, 2H, DmtNH), 8.20 (d, J = 8.8 Hz, 1H, NalNH), 8.59 (d, J = 8.4 Hz, 1H, PheNH), 9.00 (s, 1H, DmtOH).

Dmt-c[D-Lys-Phe-D-1-Nal-Asp]NH$_2$ (**4**). ^1H NMR (400 MHz, 8:2 DMSO-d_6/H$_2$O) δ: 0.64 (m, 1H, LysHγ), 0.84 (m, 1H, LysHγ), 1.04 (m, 1H, LysHβ), 1.11 (m, 1H, LysHδ), 1.23 (m, 1H, LysHδ), 1.32 (m, 1H, LysHβ), 2.13 (s, 6H, DmtMe), 2.31 (dd, J = 6.0, 13.2 Hz, 1H, PheHβ), 2.34−2.44 (m, 2H, PheHβ + AspHβ), 2.58 (dd, J = 10.2, 15.8 Hz, 1H, AspHβ), 2.80 (m, 1H, LysHε), 2.87 (m, 1H, DmtHβ), 2.92−3.00 (m, 2H, NalHβ + DmtHβ), 3.10 (m, 1H, LysHε), 3.66 (dd, J = 3.2, 14.4 Hz, 1H, NalHβ), 3.70 (m, 1H, DmtHα), 4.05 (ddd, J = 6.4, 7.6, 9.2 Hz, 1H, LysHα), 4.40−4.48 (m, 2H, PheHα + AspHα), 4.54 (ddd, J = 4.0, 9.2, 13.2 Hz, 1H, NalHα), 6.40 (s, 2H, DmtArH$_{3,5}$), 6.87−6.92 (m, 2H, PheArH), 7.09−7.12 (m, 4H, PheArH + CONH$_2$), 7.18 (d, J = 7.6 Hz, 1H, PheNH), 7.23 (s, 1H, CONH$_2$), 7.32−7.40 (m, 2H, NalArH$_{2,3}$), 7.53 (t, J = 7.2 Hz, 1H, NalArH$_6$), 7.56−7.62 (m, 2H, LysNHε + NalArH$_7$), 7.64 (d, J = 7.6 Hz, 1H, AspNH), 7.51 (d, J = 9.2 Hz, 1H, LysNH), 7.77 (d, J = 8.0 Hz, 1H, NalArH$_4$), 7.92 (d, J = 8.0 Hz, 1H, NalArH$_5$), 8.10 (d, J = 8.0 Hz, 1H, NalArH$_8$), 8.34 (m, 2H, DmtNH), 8.61 (d, J = 9.2 Hz, 1H, NalNH), 9.10 (s, 1H, DmtOH).

Dmt-c[D-Lys-Phe-D-2-Nal-Asp]NH$_2$ (**5**). ^1H NMR (400 MHz, 8:2 DMSO-d_6/H$_2$O) δ: 0.64 (m, 1H, LysHγ), 0.85 (m, 1H, LysHγ), 1.02−1.10 (m, 2H, LysHβ + LysHδ), 1.23 (m, 1H, LysHδ), 1.33 (m, 1H,

LysHβ), 2.14 (s, 6H, DmtMe), 2.35 (dd, J = 2.8, 15.6 Hz, 1H, AspHβ), 2.40–2.45 (m, 2H, PheHβ), 2.52 (dd, J = 9.2, 15.6 Hz, 1H, AspHβ), 2.79 (m, 1H, LysHε), 2.86 (m, 1H, NalHβ), 2.88 (m, 1H, DmtHβ), 2.97 (dd, J = 12.0, 13.2 Hz, 1H, DmtHβ), 3.09 (dd, J = 4.6, 13.6 Hz, 1H, NalHβ), 3.17 (m, 1H, LysHε), 3.72 (m, 1H, DmtHα), 4.08 (m, 1H, LysHα), 4.34–4.43 (m, 2H, AspHα + PheHα), 4.56 (ddd, J = 4.6, 8.8, 9.2 Hz, 1H, NalHα), 6.41 (s, 2H, DmtArH$_{3,5}$), 6.86 (d, J = 5.6 Hz, 2H, PheArH$_{2,6}$), 7.04–7.14 (m, 5H, PheArH$_{3-5}$ + CONH$_2$), 7.18 (d, J = 8.4 Hz, 1H, NalArH$_3$), 7.25 (d, J = 8.0 Hz, 1H, PheNH), 7.40–7.48 (m, 2H, NalArH$_{6,7}$), 7.52–7.56 (m, 2H, AspNH + NalArH$_1$), 7.57 (br.t, 1H, LysNHε), 7.75 (d, J = 8.8 Hz, 2H, NalArH$_8$ + LysNH), 7.79 (d, J = 8.0 Hz, 1H, NalArH$_4$), 7.83 (d, J = 8.0 Hz, 1H, NalArH$_5$), 8.31 (br.s, 2H, DmtNH), 8.43 (d, J = 9.2 Hz, 1H, NalNH), 9.13 (s, 1H, DmtOH).

4.8. 2D ROESY analyses

The experiments were conducted in DMSO-d_6/H$_2$O (8:2) in the phase-sensitive mode at room temperature, spin-locking field (γb2) was 2000 Hz, and mixing time was set to 250 ms; spectra were processed in the hypercomplex approach; peaks were calibrated on DMSO. Cross-peak intensities were classified as very strong, strong, medium, and weak, and were associated with distances of 2.3, 2.7, 3.3, and 5.0 Å, respectively (Supporting Information). The intensities of the cross peaks arising from protons separated by known distances (e.g., geminal) were found to match with these associations. Geminal and other clear correlations were discarded as constraints. For the absence of Hα(i, i + 1) ROESY cross peaks, all of the ω bonds were set at 1808 (force constant: 16 k cal mol^{-1} Å^{-2}).

4.9. Restrained molecular dynamics

Only ROESY-derived constraints were included in the MD simulations [51]. The experiments were conducted at 300 K and 1 atm by using the AMBER force field in a 30 × 30 × 30 Å box of standard TIP3P models of equilibrated water [52]. Periodic boundary conditions were applied, a dielectric constant of 1 was used, and the cut off distance for the non-bonded interactions was 12 Å. All water molecules with atoms that come closer than 2.3 Å to a solute atom were eliminated. A 100 ps simulation at 1200 K was used for generating 50 random structures that were subsequently subjected to a 50 ps restrained MD with a 50% scaled force field at the same temperature, followed by 50 ps with full restraints (distance force constant of 7 kcal mol^{-1} Å^{-2}), after which the system was cooled in 20 ps–50 K. H-bond interactions were not included, nor were torsion angle restraints. The resulting structures were minimized with 3000 cycles of steepest descent and 3000 cycles of conjugated gradient (convergence of 0.01 kcalÅ^{-1} mol^{-1}). The backbones of the structures were clustered by the rmsd analysis.

4.10. Molecular docking

The previously reported procedure [41,45], using a homology models of hMOR subsequently validated with the crystallographic structure disclosed in 2012 [2] was utilized. The initial structures of the ligands were the ROESY-derived structures of the cyclopeptides. MolDock experiments were performed with Autodock 4.0 [43], which uses an empirical scoring function based on the free energy of binding. The ligands and the MOR were further processed using the Autodock Tool Kit. Gasteiger-Marsili charges were assigned and solvation parameters were added to the final docked structure using Addsol utility. Structures with less than 1.0 A rmsd were clustered together and representative model of each cluster was selected based on the most favourable free energy of binding. Visual inspection was carried out to select the final structure. The

combined QM/MM approach, as implemented in NWChem [53] was used. The QM/MM module in NWChem was built as a top level interface between the classical MD module and various QM modules, managing initialization, data transfer, and various high level operation. For the QM/MM calculations, the ligand-receptor systems resulting from the MolDock study were first partitioned into a QM subsystem and an MM subsystem. The reaction system used a smaller QM subsystem consisting of the ligand and residues within 4.5 Å, whereas the MM subsystem was treated using a modified AMBER force field. The boundary problem between the QM and MM subsystems was treated using the pseudo-bond approach. With this QM/MM system, an iterative optimization procedure was applied to the QM/MM system, using 3-21G⁄QM/MM calculations, leading to an optimized structure for the reactants. The convergence criterion used was set to obtain an energy gradient of $<10^{-4}$, using the twin-range cut off method for non-bonded interactions, with a long-range cut off of 14 Å and a short-range cut off of 8 Å.

Author contributions

The manuscript was written through contributions of all authors. All authors have given approval to the final version of the manuscript.

Appendix A. Supplementary data

Supplementary data related to this article can be found at http://dx.doi.org/10.1016/j.ejmech.2015.12.012.

References

[1] R.J. Bodnar, Endogenous opiates and behavior: 2010, Peptides 32 (2011) 2522–2552.
[2] A. Manglik, A.C. Kruse, T.S. Kobilka, F.S. Thian, J.M. Mathiesen, R.K. Sunahara, L. Pardo, W.I. Weis, B.K. Kobilka, S. Granier, Crystal structure of the μ-opioid receptor bound to a morphinan antagonist, Nature 485 (2012) 321–326.
[3] S. Granier, A. Manglik, A.C. Kruse, T.S. Kobilka, F.S. Thian, W.I. Weis, B.K. Kobilka, Structure of the delta-opioid receptor bound to naltrindole, Nature 485 (2012) 400–404.
[4] H. Wu, D. Wacker, M. Mileni, V. Katritch, G.W. Han, E. Vardy, W. Liu, A.A. Thompson, X.P. Huang, F.I. Carroll, S.W. Mascarella, R.B. Westkaemper, P.D. Mosier, B.L. Roth, V. Cherezov, R.C. Stevens, Structure of the human kappa-opioid receptor in complex with JDTic, Nature 485 (2012) 327–332.
[5] L. He, J. Fong, M. von Zastrow, J.L. Whistler, Regulation of opioid receptor trafficking and morphine tolerance by receptor oligomerization, Cell 108 (2002) 271–282.
[6] T. Yamazaki, S. Ro, M. Goodman, N.N. Chung, P.W. Schiller, A topochemical approach to explain morphiceptin bioactivity, J. Med. Chem. 36 (1993) 708–719.
[7] A. Janecka, R. Staniszewska, J. Fichna, Endomorphin analogs, Curr. Med. Chem. 14 (2007) 3201–3208.
[8] B. Leitgeb, Structural investigation of endomorphins by experimental and theoretical methods: hunting for the bioactive conformation, Chem. Biodivers. 4 (2007) 2703–2724.
[9] L. Gentilucci, A. Tolomelli, F. Squassabia, Topological exploration of cyclic endomorphin-1 analogues, structurally defined models for investigating the bioactive conformation of MOR agonists, Protein Pept. Lett. 14 (2007) 51–56.
[10] L. Pasquinucci, O. Prezzavento, A. Marrazzo, E. Amata, S. Ronsisvalle, Z. Georgoussi, D.D. Fourla, G.M. Scoto, C. Parenti, G. Aricò, G. Ronsisvalle, Evaluation of N-substitution in 6,7-benzomorphan compounds, Bioorg. Med. Chem. 18 (2010) 4975–4982.
[11] V.J. Hruby, P.M. Balse, Conformational and topographical considerations in

designing agonist peptidomimetics from peptide leads, Curr. Med. Chem. 7 (2000) 945–970.

[12] A. Janecka, R. Kruszynski, Conformationally restricted peptides as tools in opioid receptor studies, Curr. Med. Chem. 12 (2005) 471–481.

[13] L. Gentilucci, R. De Marco, L. Cerisoli, Chemical modifications designed to improve peptide stability: incorporation of non-natural amino acids, pseudo-peptide bonds, and cyclization, Curr. Pharm. Des. 16 (2010) 3185–3203.

[14] A. Keresztes, A. Borics, G. Tóth, Recent advances in endomorphin engineering, ChemMedChem 5 (2010) 1176–1196.

[15] L. Gentilucci, A. Tolomelli, R. De Marco, R. Artali, Molecular docking of opiates and opioid peptides, a tool for the design of selective agonists and antagonists, and for the investigation of atypical ligand-receptor interactions, Curr. Med. Chem. 19 (2012) 1587–1601.

[16] R. Perlikowska, J.C. do-Rego, A. Cravezic, J. Fichna, A. Wyrebska, G. Tóth, A. Janecka, Synthesis and biological evaluation of cyclic endomorphin-2 analogs, Peptides 31 (2010) 339–345.

[17] J. Fichna, R. Perlikowska, A. Wyrebska, K. Gach, J. Piekielna, J.C. do-Rego, G. Tóth, A. Kluczyk, T. Janecki, A. Janecka, Effect of 2′,6′-dimethyl-L-tyrosine (Dmt) on pharmacological activity of cyclic endomorphin-2 and morphiceptin analogs, Bioorg. Med. Chem. 19 (2011) 6977–6981.

[18] R. Perlikowska, J. Piekielna, J. Fichna, J.C. do-Rego, G. Tóth, T. Janecki, A. Janecka, Pharmacological properties of novel cyclic pentapeptides with μ-opioid receptor agonist activity, Med. Chem. 10 (2014) 154–161.

[19] R. Perlikowska, D. Malfacini, M.C. Cerlesi, G. Calo, J. Piekielna, L. Floriot, T. Henry, J.C. do-Rego, C. Tömböly, A. Kluczyk, A. Janecka, Pharmacological characterization of endomorphin-2-based cyclic pentapeptides with methyl-ated phenylalanine residues, Peptides 55 (2014) 145–150.

[20] J. Piekielna, L. Gentilucci, R. De Marco, R. Perlikowska, A. Adamska, J. Olczak, M. Mazur, R. Artali, J. Modranka, T. Janecki, C. Tomboly, A. Janecka, Cyclic side-chain-linked opioid analogs utilizing cis- and trans-4-aminocyclohexyl-D-alanine, Bioorg. Med. Chem. 22 (2014) 6445–6451.

[21] J. Piekielna, R. Perlikowska, J.C. do-Rego, J.L. do-Rego, M.C. Cerlesi, G. Calo, A. Kluczyk, K. Łapiński, C. Tömböly, A. Janecka, Synthesis of mixed opioid affinity cyclic endomorphin-2 analogues with fluorinated phenylalanines, ACS Med. Chem. Lett. 6 (2015) 579–583.

[22] Y. Sasaki, T. Suto, A. Ambo, H. Ouchi, Y. Yamamoto, Biological properties of opioid peptides replacing Tyr at position 1 by 2,6- dimethyl-Tyr, Chem. Pharm. Bull. (Tokyo) 47 (1999) 1506–1509.

[23] Y. Okada, Y. Fujita, T. Motoyama, Y. Tsuda, T. Yokoi, T.Y. Li, Y. Sasaki, A. Ambo, Y. Jinsmaa, S.D. Bryant, L.H. Lazarus, Structural studies of [2′,6′-dimethyl-L-tyrosine[1]]endomorphin-2 analogues: enhanced activity and cis orientation of the Dmt-Pro amide bond, Bioorg. Med. Chem. 11 (2003) 1983–1994.

[24] C. Yue, J. Thierry, P. Potier, 2-phenyl isopropyl esters as carbonyl terminus protecting groups in the fast synthesis of peptide fragments, Tetrahedron Lett. 34 (1993) 323–326.

[25] A. Aletras, K. Barlos, D. Gatos, S. Koutsogianni, P. Mamos, Preparation of the very acid-sensitive Fmoc-Lys(Mtt)-OH application in the synthesis of side-chain to side-chain cyclic peptides and oligolysine cores suitable for the solid-phase assembly of MAPs and TASPs, Int. J. Pept. Protein Res. 45 (1995) 488–496.

[26] M. Katsara, T. Tselios, S. Deraos, G. Deraos, M.T. Matsoukas, E. Lazoura, J. Matsoukas, V. Apostolopoulos, Round and round we go: cyclic peptides in disease, Curr. Med. Chem. 13 (2006) 2221–2232.

[27] Y.-C. Cheng, W.H. Prusoff, Relationships between the inhibition constant (Ki) and the concentration of inhibition which cause50% inhibition (IC50) of an enzymatic reaction, Biochem. Pharmacol. 22 (1973) 3099–3108.

[28] V. Camarda, G. Calo, Chimeric G proteins in fluorimetric calcium assays: experience with opioid receptors, Methods Mol. Biol. 937 (2013) 293–306.

[29] V. Camarda, C. Fischetti, N. Anzellotti, P. Molinari, C. Ambrosio, E. Kostenis, D. Regoli, C. Trapella, R. Guerrini, S. Salvadori, G. Calo, Pharmacological profile of NOP receptors coupled with calcium signaling via the chimeric protein Gαqi5, Naunyn Schmiedeb. Arch. Pharmacol. 379 (2009) 599–607.

[30] A. Pfeiffer, V. Brantl, A. Herz, H.M. Emrich, Psychotomimesis mediated by κ opiate receptors, Science 233 (1986) 774–776.

[31] N.K. Mello, S.S. Negus, Interactions between kappa opioid agonists and cocaine-preclinical studies, New medications for drug abuse, Ann. N.Y. Acad.

Sci. 909 (2000) 104–132.

[32] A. Barber, R. Gottschlich, Novel developments with selective, non-peptidic kappa-opioid receptor agonists, Exp. Opin. Investig. Drugs 6 (1997) 1351–1368.

[33] D.L. DeHaven-Hudkins, R.E. Dolle, Peripherally restricted opioid agonists as novel analgesic agents, Curr. Pharm. Des. 10 (2004) 743–757.

[34] B.M. Greedy, F. Bradbury, M.P. Thomas, K. Grivas, G. Cami-Kobeci, A. Archambeau, K. Bosse, M.J. Clark, M. Aceto, J.W. Lewis, J.R. Traynor, S.M. Husbands, Orvinols with mixed kappa/mu opioid receptor agonist activity, J. Med. Chem. 56 (2013) 3207–3216.

[35] S.S. Negus, N.K. Mello, Effects of kappa opioid agonists on cocaine self-administration under a progressive ratio schedule in rhesus monkeys, Drug Alcohol Depend. 63 (2001) S113.

[36] A. Greco, S. Tani, R. De Marco, L. Gentilucci, Synthesis and analysis of the conformational preferences of 5-aminomethyloxazolidine-2,4-dione scaffolds: first examples of β2-and β2,2-homo-freidinger lactam analogues, Chem. Eur. J. 20 (2014) 13390–13404.

[37] P.A. Temussi, D. Picone, G. Saviano, P. Amodeo, A. Motta, T. Tancredi, S. Salvadori, R. Tomatis, Biopolymers 32 (1992) 367–372 (and references herein).

[38] A. Borics, G. Tóth, Structural comparison of mu-opioid receptor selective peptides confirmed four parameters of bioactivity, J. Mol. Graph. Model 28 (2010) 495–505.

[39] C. Toniolo, Intramolecularly hydrogen-bonded peptide conformations, CRC Crit. Rev. Biochem. 9 (1980) 1–44.

[40] W.D. Cornell, P. Cieplak, C.I. Bayly, I.R. Gould, K.M. Merz, D.M. Ferguson, D.C. Spellmeyer, T. Fox, J.W. Caldwell, P.A. Kollman, A second generation force field for the simulation of proteins and nucleic acids, J. Am. Chem. Soc. 117 (1995) 5179–5197.

[41] L. Gentilucci, A. Tolomelli, R. De Marco, S. Spampinato, A. Bedini, R. Artali, The inverse type II β-Turn on D-Trp-Phe, a pharmacophoric motif for MOR agonists, ChemMedChem 6 (2011) 1640–1653.

[42] H. Kessler, Conformation and biological activity of cyclic peptides, Angew. Chem. Int. Ed. Engl. 21 (1982) 512–523.

[43] G.M. Morris, D.S. Goodsell, R.S. Halliday, R. Huey, W.E. Hart, R.K. Belew, A.J. Olson, Automated docking using a lamarckian genetic algorithm and empirical binding free energy function, J. Comput. Chem. 19 (1998) 1639–1662.

[44] C.B. Fowler, I.D. Pogozheva, A.L. Lomize, H. LeVine III, H.I. Mosberg, Complex of an active μ-opioid receptor with a cyclic peptide agonist modeled from experimental constraints, Biochemistry 43 (2004) 15796–15810.

[45] L. Gentilucci, F. Squassabia, R. Demarco, R. Artali, G. Cardillo, A. Tolomelli, S. Spampinato, A. Bedini, Investigation of the interaction between the atypical agonist c[YpwFG] and MOR, FEBS J. 275 (2008) 2315–2337.

[46] I.D. Pogozheva, M.J. Przydzial, H.I. Mosberg, Homology modeling of opioid receptor-ligand complexes using experimental constraints, AAPS J. 7 (2005) E434–E448.

[47] T. Vojkovsky, Detection of secondary amines on solid phase, Pept. Res. 8 (1995) 236–237.

[48] B.R. Conklin, Z. Farfel, K.D. Lustig, D. Julius, H.R. Bourne, Substitution of three amino acids switches receptor specificity of Gqα to that of Giα, Nature 363 (1993) 274–276.

[49] E. Kostenis, L. Martini, J. Ellis, M. Waldhoer, A. Heydorn, M.M. Rosenkilde, P.K. Norregaard, R. Jorgensen, J.L. Whistler, G. Milligan, A highly conserved glycine within linker I and the extreme C terminus of G protein α subunits interact cooperatively in switching G protein-coupled receptor-to-effector specificity, J. Pharmacol. Exp. Ther. 313 (2005) 78–87.

[50] N.B. Eddy, D. Leimbach, Synthetic analgesics II. Dithienylbutenyl- and dithienylbutylamines, J. Pharmacol. Exp. Ther. 107 (1953) 385–393.

[51] HyperChem, Release 8.0.3, Hypercube Inc., 1115 NW 4th St. Gainesville, FL 32608, USA, 2007.

[52] W.L. Jorgensen, J. Chandrasekhar, J. Madura, R.W. Impey, M.L. Klein, Comparison of simple potential functions for simulating liquid water, J. Chem. Phys. 79 (1983) 926–935.

[53] NWChem: Open source high-performance computational chemistry. http://www.nwchem-sw.org/index.php/Main_Page.